NUMERICAL SIMULATION OF

TRADITIONAL AND TECHNOLOGICAL ZINC-BASED COATINGS: PART I

Sabrina Vantadori[1], Andrea Zanichelli[1], Camilla Ronchei[2],

Daniela Scorza[3], Vittorio Di Cocco[4], Francesco Iacoviello[4]

[1]Department of Engineering & Architecture, University of Parma,
Parco Area delle Scienze 181/A, 43124 Parma, Italy

[2]Department of Civil Engineering, University of Calabria,
via Pietro Bucci, 87036 Arcavacata di Rende (CS), Italy

[3]Department of Engineering, University of Naples Parthenope,
Centro Direzionale Isola C4, 80143 Napoli, Italy

[4] DICeM, Università di Cassino e del Lazio Meridionale,
Via G. Di Biasio, 43, 03043 Cassino (FR), Italy

Abstract

In the present paper, the bending behaviour of a hot-rolled hyper-sandelin steel subjected to hot-dip galvanising (HDG) is numerically simulated. Two coating types are analysed, that is: a pure zinc coating and a zinc-based coating with 3% Sn addition by weight.

It was experimentally observed that the tin addition influences the thickness of each intermetallic phase and increases the ductility

of the intermetallic phases. Therefore, the key of the numerical simulation is to assume suitable constitutive laws to phase layers, by considering that only few mechanical parameters are available in the literature.

Such an approach has shown quite satisfactory results and it can be promising as a numerical tool to be used by HDG industry, being quite simple but quite accurate to estimate flexural strength and damage of Zn-based coated steels.

Keywords

Bath; dipping time; HDG; technological coating; zinc-based coatings

1. INTRODUCTION

Hot-dip galvanising (HDG) is a widely used technique to protect structural steel, due to its inherent capacity to long-lasting without requiring any maintenance **[1-4]**.

Such a technique consists in the formation of a protective layer of zinc on the surface of steel. In turn, zinc oxidises but with a rate much lower with respect to uncoated steel. As a matter of fact, the zinc-consummation rate in a normal urban environment is of the order of 1 µm per year (up to 2µm per year in the case of polluted environment) and this is equivalent to state that the duration of the protection by HDG would be even beyond 50 years, considering an average zinc thickness which is often times higher than the minimum one prescribed by the UNI EN ISO 1461 standard **[5]**.

Therefore, a zinc coating protects steel with a double mechanism **[6]**, that is: (i) by a barrier effect, interposing itself between the steel surface and the aggressive atmosphere (passive protection) being perfectly continuous and impact resistant; (ii) by a cathodic protection, corroding itself instead of steel, due to the different electromechanical potential of these two materials (active protection). It is worth noting that, the (ii) effect ensures that, in the case of nicks, scratches, and small uncoated regions, the surrounding zinc corrodes itself instead of steel. Moreover, the corrosion products tend to seal the above defects, preventing oxygen and other aggressive elements of coming into contact with uncoated steel, holding up the degradation process. By the way, the zinc in atmosphere tends to cover itself with a thin stable layer of oxides

and carbonates (passivation layer) that protects it from dissolution, determining the long duration of steel protection.

When the steel is dipped in the zinc bath (molten zinc at a temperature equal to about 450°C), a series of zinc-iron alloy layers (intermetallic phases) is formed with different chemical compositions of the above two metals. This is not a chemical reaction but, instead, a physical process or metallurgical reaction. As a matter of fact, the growth of a hot-dip galvanizing coating is due to the interdiffusion of zinc and iron atoms between the zinc melting and steel surface.

The intermetallic phases, that grow during the dipping in the zinc bath, are well characterised and recognisable both in terms of chemical composition and morphology of microstructure **[7]**. As a matter of fact, each of them corresponds to one of the homogeneous phases in the zinc-iron phase diagram (**Figure 1**), where the content of zinc in the coating increases by moving from the inner zone to the outer zone, whereas the iron content decreases by moving from the inner zone to the outer zone.

In a typical zinc coating, the following intermetallic phases are recognisable **[7]** and, by starting from the steel substrate, they are (**Figure 2**):

- the Γ phase, consisting in a layer of about 1μm in thickness, characterised by a zinc (Zn) content of about 70% by weight and an iron (Fe) content ranging between 26.8% and 31.1% by weight. The phase is characterised by a face-centred cubic atoms arrangement;

- the δ phase, characterised by an iron content of the order of 10% by weight and by a hexagonal crystal structure;

- the ζ phase, characterised by an iron content of about 7% by weight. It is an isomorphous phase, characterised by a monoclinic unit cell and an atomic structure that contains a Fe atom and a Zn atom, surrounded by 12 Zn atoms at the vertices of a slightly distorted icosahedron. Such icosahedra are linked together to form chains, organised in a hexagonal array **[8]**;

- the η phase, characterised by a chemical composition quite similar to that of the bath, with a maximum iron content up to 0.03% by weight. When the bath consists of a technological zinc alloy (for example by adding tin and nickel), such a phase will be influenced by the presence of the above chemical elements.

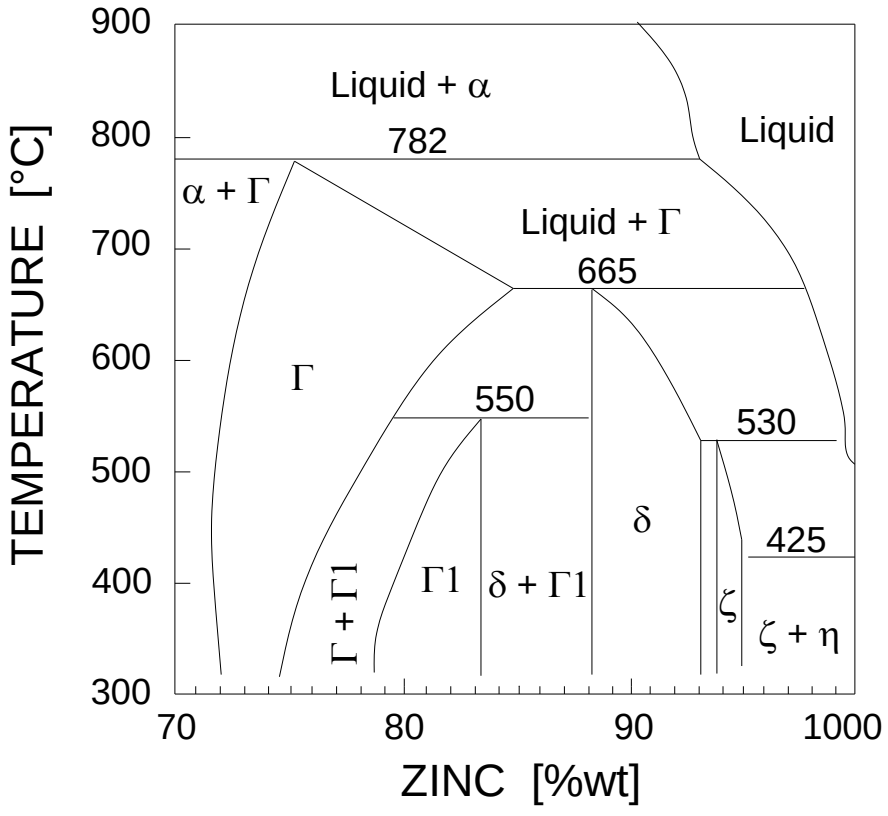

Figure 1. Zinc-iron phase diagram.

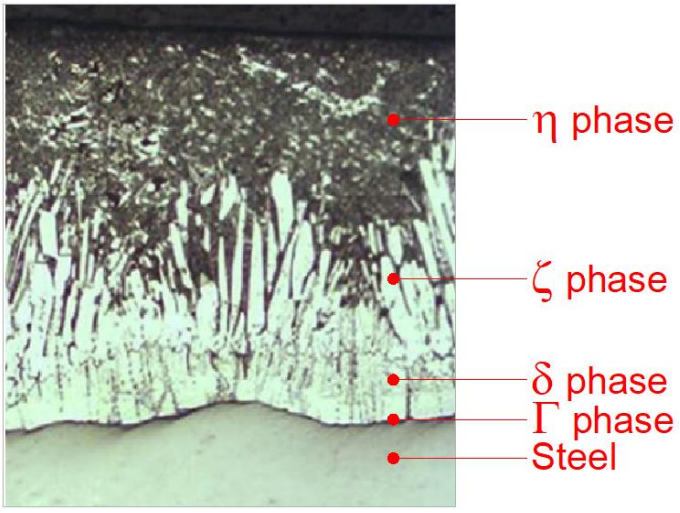

Figure 2. Typical zinc coating intermetallic phases: Γ, δ, ζ and η phase.

The fact that coating is composed by layers with different chemical compositions and morphologies of microstructure produces a variability of the mechanical properties along the coating thickness. As a matter of fact: the elastic modulus ranges from 75 GPa (in correspondence to η phase) to 140 GPa (in correspondence to δ phase), whereas the micro-hardness ranges from 70VHN (η phase) to 280 VHN (δ phase) **[9]**. Therefore, the outer phases are characterised by ductility and high attitude to plastic deformation **[9]**, whereas the inner phases are characterised by lower ductility **[10]**. Moreover, the η phase is soften and able to absorb impact, whereas the more inner phases, characterised by a high micro-hardness, give to galvanised steel advantages in terms of wear resistance and toughness.

Moreover, it is worth noting that the adherence of the coating to the steel support is guaranteed by the formation mechanics, that is

the interdiffusion of Zn atoms and Fe atoms **[9]**. Such a mechanics produces evident benefits with respect to other anticorrosive treatments that employ metals overlapping (as, for example, in the electroplating and metallisation processes) or organic coating (as, for example, liquid or powder paints).

In the last years, there has been an increasing research on zinc coatings, in order to optimise the phases thickness and the mechanical and physical performances **[7]**. Such a research has to inevitably take into account the factors that influence the formation mechanics, and more precisely **[11]**:

- the temperature and bath composition;
- the dipping time;
- the composition and the superficial state of the steel.

About the bath temperature, the operation conditions are usually between 440°C and 460°C. However, for technical zinc-based coatings, high temperature baths, up to 550°C, are possible. The formation of the ζ phase does not take place, and therefore the coating is composed by δ and η phases. At such high temperatures, thicknesses greater than 100μm are difficult to be reached.

About the bath composition, generally the zinc bath is pure at 98% (as required by the UNI EN ISO 1461 standard **[5]**). A very small amount of other metals can be present, added as technological components of the alloy or as zinc impurities. In the context of technological zinc alloys mainly nickel, aluminium, strontium, tin, bismuth and magnesium are added. For examples, the addition of nickel into the bath delays the growth of δ phase. Thus, zinc-based

coating holds superior performance in terms of corrosion resistance, weldability, adherence, uniform thickness and good paintability with respect to pure zinc coating **[12-15]**. On the other hand, corrosion resistance and adherence can be improved by strontium addition **[16]**.

About the dipping time, it is generally between 1.5 and 5 minutes. In the first minutes, the greatest growth of the coating thickness occurs. Clearly, the steel thickness plays a decisive role to determine the dipping time inside the bath.

About the composition of the steel, the addition of other elements to iron and carbon in the alloy leads to an increasing or decreasing of the growth of coating thickness. More precisely, the additions that strongly influence such a growth are the silicon and the phosphorus. As a matter of fact, it was experimentally observed that a content of silicon between 0.03% and 0.12% in weight (sandelin range) or higher than 0.25% in weight (hyper-sandelin steels) is able to accelerate the Zn-Fe diffusion, resulting in coatings characterised by high thickness **[17]**. Moreover, the combined effect of silicon and phosphorus amplifies the sandelin effect.

Also the steel state can influence the coating thickness, and more precisely its surface roughness, due to both the carry-over effects and the increased specific surface.

In the present paper, the bending behaviour of a HD galvanised hot-rolled hyper-sandelin steel is numerically simulated by considering both a pure zinc coating and a zinc-based coating with 3% Sn addition in weight, that is a technological coating. More precisely, the proposed numerical models aim to simulate some

experimental bending tests available in the literature **[18-21]**, performed by considering, for each of the aforementioned baths, five different dipping time values. The numerical models, developed by using the Finite Element Method, exploit the experimental observations of the longitudinal section of the specimens at the end of the bending tests, performed by light optical microscope, in terms of intermetallic phase thickness, morphology and damage.

The paper is organised as follows. **Section 2** is dedicated to the experimental campaign description, in terms of specimens, baths composition, dipping times, testing machine used and obtained results. **Section 3** is aimed to the numerical models description. Numerical results are presented in **Section 4** and compared with the experimental ones. Conclusions are summarised in **Section 5.**

2. EXPERIMENTAL CAMPAIGN

The experimental tests **[18-21]** were performed on HD galvanised specimens under constant bending moment, applied by means of a non-standardised device **[10].** The longitudinal sections of the specimens were experimentally observed by LOM to measure both the phases thicknesses (before testing) and the level of damage (after testing) **[22,23].**

The specimens, manufactured from hot-rolled hyper-sandelin steel plates, had the geometrical configuration shown in **Figure 3.**

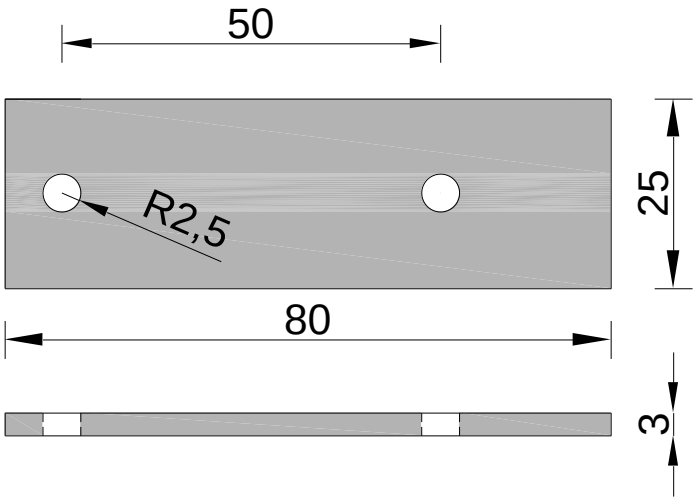

Figure 3. Geometrical configuration of the steel specimen. Sizes in mm.

The chemical composition is reported in **Table 1.**

Table 1. Chemical composition of the steel support (wt%).

C	Si	Mn	P	S	Al	Fe
0.090	0.167	0.540	0.010	0.004	0.051	Bal.

The galvanised process was preceded by the preparation of steel support. More precisely, firstly, the surface was degreased and rinsed by using alcohol. Then, the specimen was pickled in an aqueous solution of hydrochloric acid (50%) for 10 minutes at room temperature, washed in fresh water (20°C) and fluxed in an aqueous solution of zinc chloride (280g/l) and ammonium chloride (220g/l) for 2 minutes at room temperature. Finally, the specimen was dried (50°C) for 10 minutes.

The coating was performed at 460 ± 2°C by using two different baths:

- a pure zinc bath;

- a technological bath, obtained by employing a tin addition (3% Sn in weight).

Five different dipping time were considered, that is: 15, 60, 180, 360 and 900s.

The experimental observations of coating sections performed by LOM allowed to identify the coatings kinetic and to measure the thickness of each intermetallic phase, as reported in **Table 2**.

Table 2. Thickness of the intermetallic phases: pure zinc bath and technological bath by varying the dipping time.

DIPPING TIME [s]	**PHASE**	**PURE Zn B.** [μm]	**TECHN. B.** [μm]
15	δ	13.000	14.946
	ζ	4.000	19.456
	η	9.000	21.679
60	δ	16.720	16.318
	ζ	9.753	20.138
	η	43.193	25.034
180	δ	10.987	12.882
	ζ	75.166	36.208
	η	15.846	26.928
360	δ	18.337	14.905
	ζ	139.674	51.777
	η	21.990	31.296
900	δ	11.757	34.065
	ζ	150.213	75.951
	η	28.030	46.772

The bending tests were performed by the non-standardised device shown in **Figure 4**, represented by a double symmetrical articulated mechanism. The specimen, containing two holes (**Figure 3**), was clamped by two gripping heads. The tests were performed under the displacement control of the crosshead. The force P and the bending

angle were measured and registered during testing. The feature of such a device was to apply a constant bending moment along the calibrated length of the specimen (**Figure 3**). The test was stopped at a crosshead displacement equal to 35 mm.

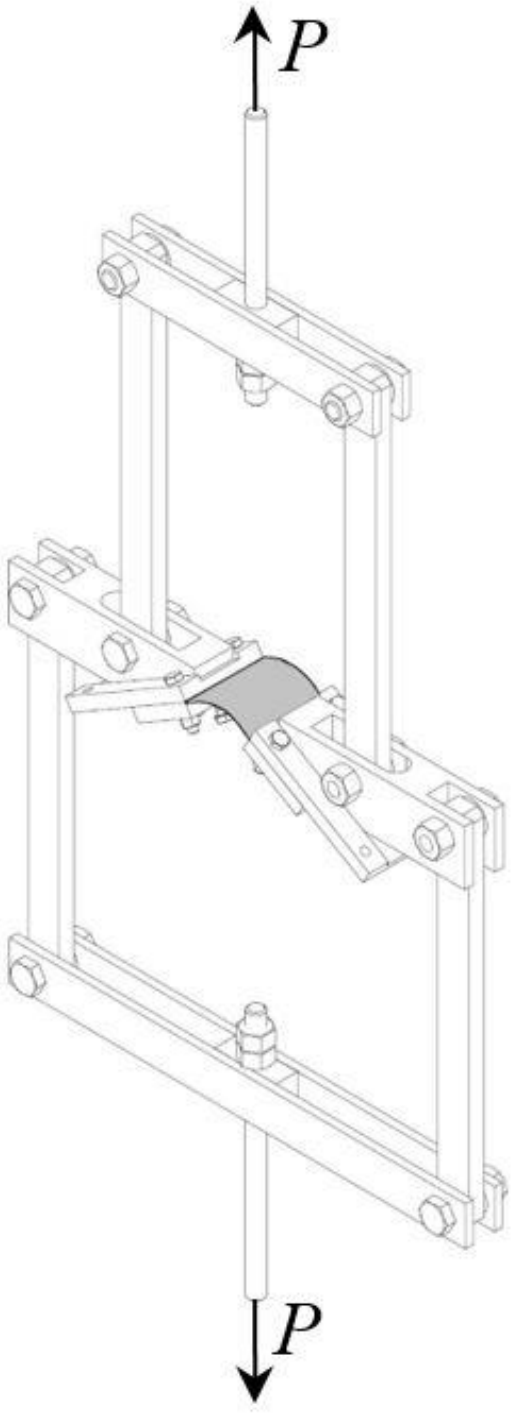

Figure 4. Non-standardised device employed to perform the bending tests.

The curve of bending moment against half bending angle is reported in **Figure 5** for each dipping time and for the two coatings employed.

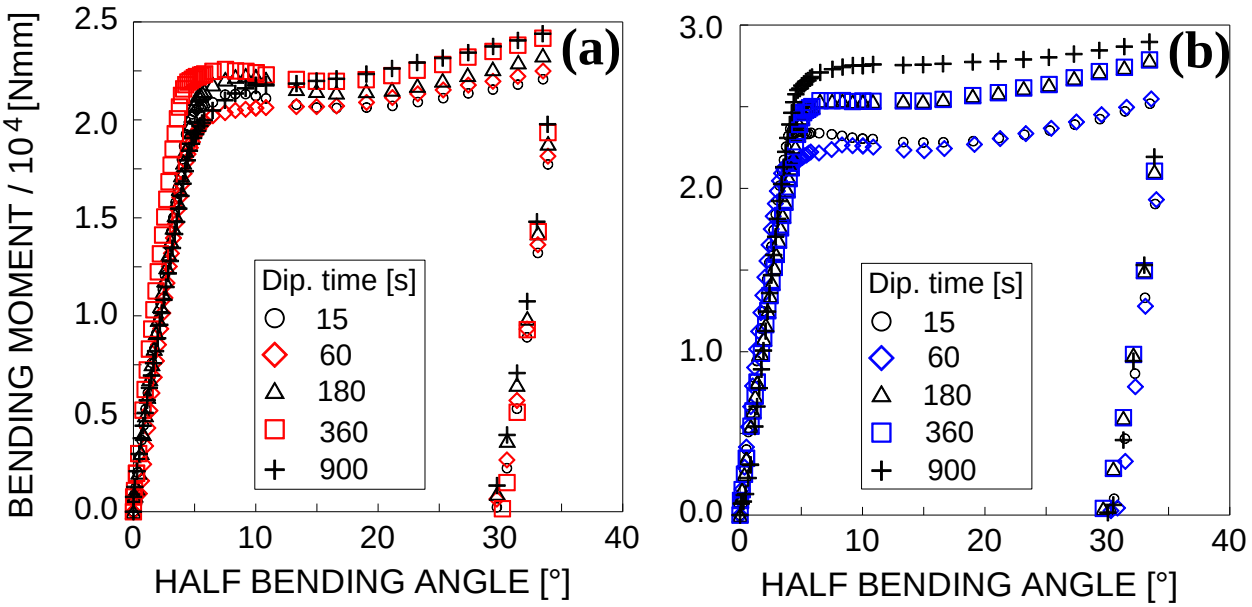

Figure 5. Bending moment vs. half bending angle for each dipping time examined, in the case of:
(a) pure zinc bath and (b) technological bath.

For both coatings it can be observed that, for a given value of the half bending angle, the bending moment increases by increasing the dipping time (up to 11% for the pure zinc coating and to 15% for the zinc-based coating, with respect to a dipping time equal to 15s) and that, for a given value of dipping time, the reached bending moment, in the case of technological coating, was greater with respect to the pure zinc coating.

After the testing, the longitudinal section of the specimen was observed by means of the LOM, where the specimen was metallographically prepared and etched by using nital at 1% for 10s.

The metallographies obtained at the end of the testing are reported in **Appendix A** for each dipping time and for both the coatings

examined. Due to the fact that the compressive side was characterised by a negligible damage, only the tensile side is reported in **Appendix A** for each specimen examined. Mainly radial cracks were observed on such a side, both for the pure zinc and the technological coating, and more precisely: it was observed that the cracks nucleated at the coating-support interphase. Then, different crack paths were followed, that is: (i) crack propagated in δ phase and arresting at the δ-ζ interphase; (ii) crack propagated both in δ and ζ phases, arresting in ζ phase; (iii) crack propagated both in δ and ζ phases, arresting in ζ-η interphase. It is worth noting that no crack propagation was observed in η phase. Only for high values of dipping time, the presence of some longitudinal cracks was observed.

In order to quantify the damage inside the intermetallic phases, the radial cracks density (cracks No./length) was calculated by counting the number of cracks present on the tensile side, and measured along a length equal to 1mm. This operation was repeated 6 times on each metallography examined. In **Figure 6**, the radial cracks density at the end of the testing is plotted against the dipping time for both the pure zinc bath and the technological bath.

It can be observed that the mechanical behaviour of the specimens coated by using a technological bath is more ductile with respect to those coated by a pure zinc bath for each dipping time examined, due to the ductility of all the intermetallic phases that characterise the zinc-based coating. Moreover, the best galvanising

condition was obtained for a dipping time equal to 60s for both baths.

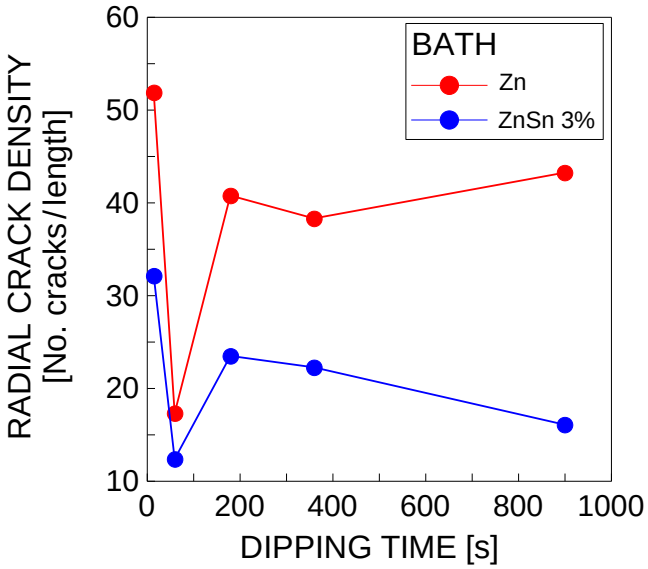

Figure 6. Radial crack density vs. dipping time in the case of pure zinc bath (Zn) and technological bath (ZnSn 3%).

3. NUMERICAL MODELS

The Finite Element Method (FEM) is used to numerically simulate the behaviour of coated specimens, tested according to the procedure described in **Section 2.** A commercial FE modelling software package (Straus 7, G+D Computing, Sydney, Australia) is used.

Two numerical models are developed, and more precisely:

- Model A, used to simulate the specimens galvanised by a pure zinc bath;
- Model B, used to simulate the specimens galvanised by a zinc-based bath with an addition of 3% by weight of tin.

The difference between the above models consists in the laws used to simulate the behaviour of intermetallic phases, due to the fact

that in the technological coating all phases experimentally showed a ductile behaviour, whereas in the pure zinc coating only the η phase showed a ductile behaviour.

The geometry of the steel specimen is reported in **Figure 3**, although for the sake of modelling only the calibrated length is considered, and equal to 50mm. Each intermetallic phase, observed during the experimental campaign, is modelled as a single layer, whose thicknesses are listed in **Table 2**. Perfect adherence is assumed between each layer, due to the fact that mainly radial cracks were experimentally observed.

Since each specimen is in a plane strain condition, a 2D FE model is developed and, due to the symmetry of the problem, only one-half of the specimen is modelled (**Figure 7**). The boundary condition applied on the symmetric axis consists in displacement along x_1 axis and the rotation around x_3 axis equal to zero for all nodes on such an axis (**Figure 7**). In order to simulate the testing condition, represented by the imposed displacement of the crosshead of testing machine, an imposed rotation along the border line of the model, characterised by $x_1 = 25mm$, is applied (**Figure 7**). The aforementioned boundary conditions allow to achieve a constant bending moment in all sections of the numerical model, that is the same loading condition characterising the tested specimens.

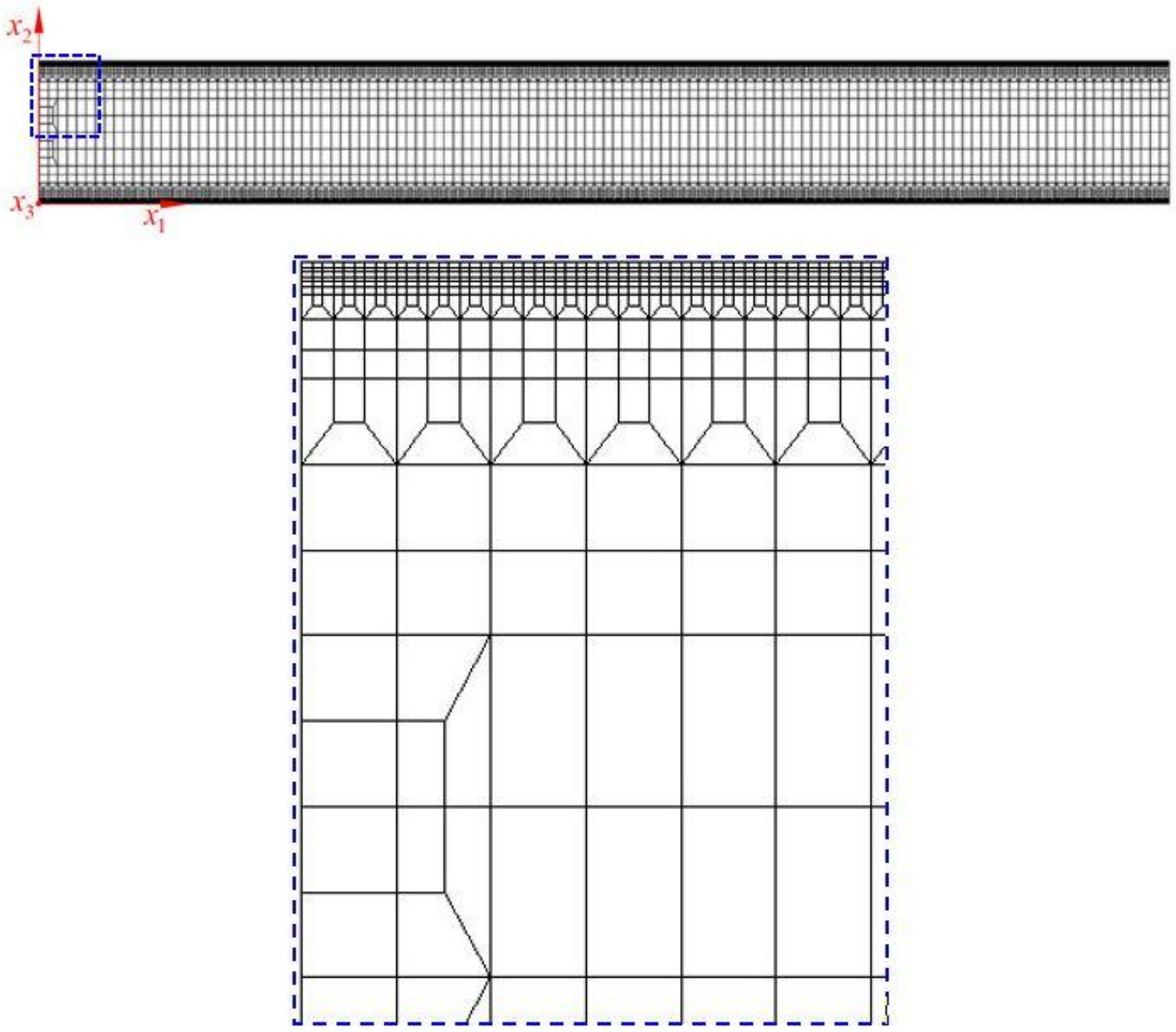

Figure 7. FE model and reference frame $x_1x_2x_3$.

The discretisation employed is shown in **Figure 7**. The type and the number of the FEs used are listed in **Table 3** for the model A and in **Table 4** for the model B, together with the nodes No. and the FE minimum size.

The FE analysis is a non-linear static one.

Table 3. Model A: type and No. of FEs, No. of nodes and minimum size of the FE employed for each dipping time examined.

MODEL A	Dip. time [s]	FEs type	FEs No.	Nodes No.	Min. FE size [mm]
Steel	-	Quad4	6252	7351	$2.31 \cdot 10^{-2}$
δ phase	15	Quad4	2160	4324	$1.30 \cdot 10^{-2}$
	60		2160	4324	$1.67 \cdot 10^{-2}$
	180		2160	4324	$1.10 \cdot 10^{-2}$
	360		4320	6482	$9.17 \cdot 10^{-3}$
	900		2160	4324	$1.18 \cdot 10^{-2}$
ζ phase	15	Quad4	2160	4324	$4.00 \cdot 10^{-3}$
	60		2160	4324	$9.75 \cdot 10^{-3}$
	180		10800	12972	$1.50 \cdot 10^{-2}$
	360		21600	23782	$1.40 \cdot 10^{-2}$
	900		25920	28106	$1.25 \cdot 10^{-2}$
η phase	15	Quad4	2160	4324	$9.00 \cdot 10^{-3}$
	60		8640	10810	$1.08 \cdot 10^{-2}$
	180		2160	4324	$1.58 \cdot 10^{-2}$
	360		4320	6482	$1.10 \cdot 10^{-2}$
	900		4320	6482	$1.40 \cdot 10^{-2}$

Table 4. Model B: type and No. of FEs, No. of nodes and minimum size of the FE employed for each dipping time examined.

MODEL A	Dip. time [s]	FEs type	FEs No.	Nodes No.	Min. FE size [mm]
Steel	-	Quad4	6252	7351	$2.31 \cdot 10^{-2}$
δ phase	15	Quad4	2160	4324	$1.49 \cdot 10^{-2}$
	60		2160	4324	$1.63 \cdot 10^{-2}$
	180		2160	4324	$1.29 \cdot 10^{-2}$
	360		2160	4324	$1.49 \cdot 10^{-2}$
	900		4320	6482	$1.70 \cdot 10^{-2}$
ζ phase	15	Quad4	4320	6482	$9.73 \cdot 10^{-3}$
	60		2160	4324	$2.01 \cdot 10^{-2}$
	180		6480	8648	$1.21 \cdot 10^{-2}$
	360		6480	8648	$1.73 \cdot 10^{-2}$
	900		10800	12972	$1.52 \cdot 10^{-2}$
η phase	15	Quad4	4320	6482	$1.08 \cdot 10^{-2}$
	60		2160	4324	$2.31 \cdot 10^{-2}$
	180		4320	6482	$1.35 \cdot 10^{-2}$
	360		4320	6482	$1.56 \cdot 10^{-2}$
	900		6480	8648	$1.56 \cdot 10^{-2}$

3.1 Model A: constitutive laws

The parameters that characterise the mechanical behaviour of the steel and the intermetallic phases are listed in **Table 5.**

Table 5. Mechanical parameters of the steel and intermetallic phases for both Model A and B.

MATERIAL / PHASE	Ref.	E [GPa]	$\sigma_{y,H}$ [MPa]	$\sigma_{y,S}$ [MPa]	σ_{max} [MPa]	σ_u [MPa]	$\frac{\varepsilon_0}{10^{-3}}$	$\frac{\varepsilon_s}{10^{-3}}$	$\frac{\varepsilon_i}{10^{-2}}$	$\frac{\varepsilon_r}{10^{-2}}$	$\frac{\varepsilon_u}{10^{-1}}$	$\frac{\varepsilon_c}{10^{-3}}$
Steel	**[21]**	210	450	400	588	533	4.60	5.60	2.16	5.92	1.11	-
η phase	**[9]**	75	210	-	-	-	-	-	-	-	-	-
MODEL A												
δ phase	**[9]**	140	450	-	-	-	-	-	-	-	-	3.21
ζ phase	**[21]**	107.5	210	-	-	-	-	-	-	-	-	2.25
MODEL B												
δ phase	**[9]**	140	450	-	-	-	-	-	-	-	-	-
ζ phase	**[21]**	107.5	450	-	-	-	-	-	-	-	-	-

The stress-strain curve for the steel under tension is typical of an elasto-plastic with strain hardening material, whereas under compression is elastic (**Figure 8(a)**).

The stress-strain curve for the δ phase is typical of an elastic material, with a tension cut-off (**Figure 8(b)**).

The stress-strain curve for the ζ phase is typical of an elastic material, with a tension cut-off (**Figure 8(b)**).

The stress-strain curve for the η phase is typical of an elasto-perfectly plastic material under tension, whereas under compression is elastic (**Figure 8(c)**).

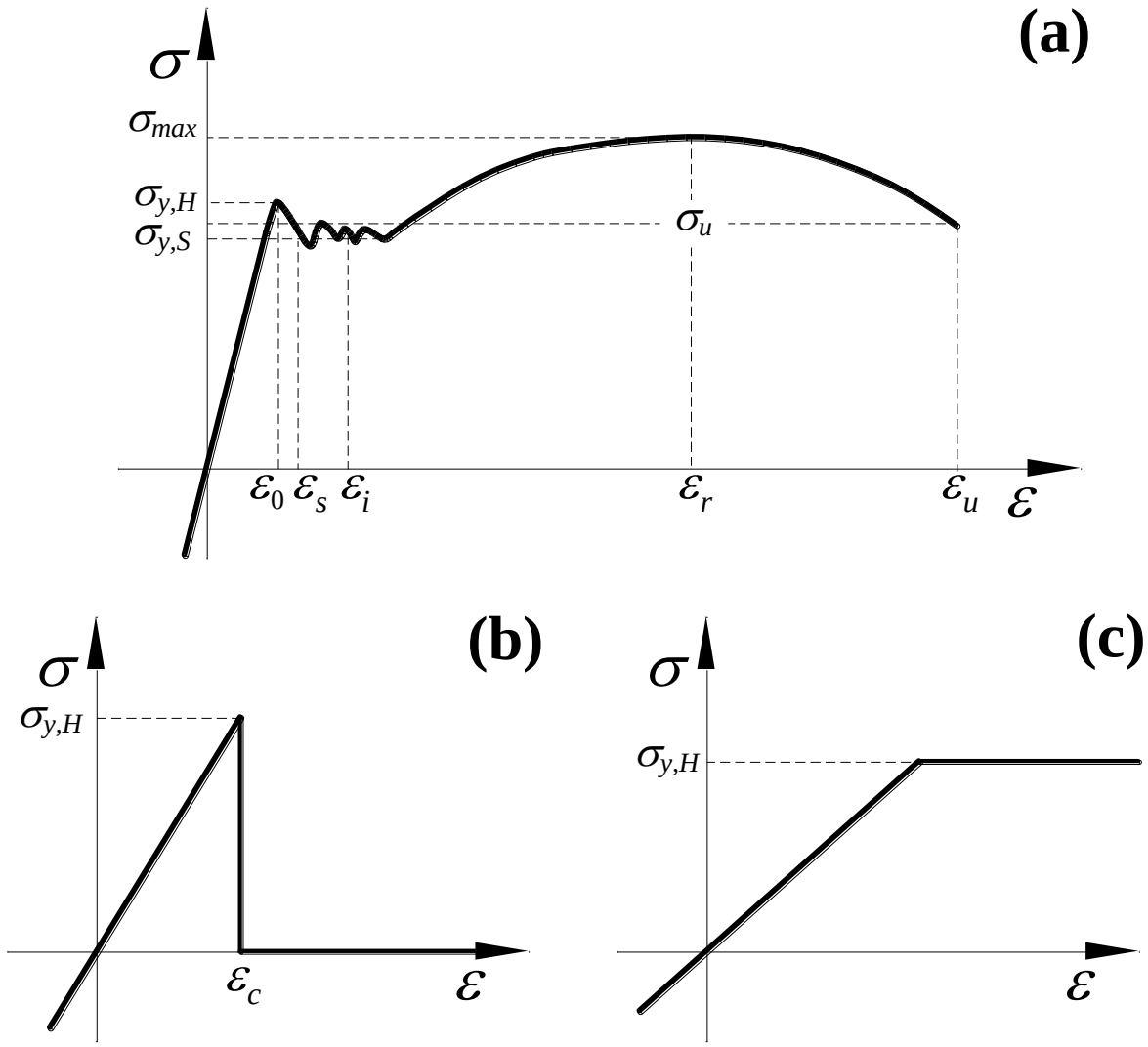

Figure 8. Stress strain curves employed in the numerical modelling: (a) elasto-plastic with strain hardening, (b) elastic material with cut-off, and (c) elasto-perfectly plastic.

3.2 Model B: constitutive laws

The parameters that characterised the mechanical behaviour of the steel and intermetallic phases are listed in **Table 5**.

The stress-strain curve for the steel is that previously presented for the Model A (**Figure 8(a)**).

The stress-strain curve for the δ, ζ and η phase is typical of an elasto-perfectly plastic material under tension, whereas under compression is elastic (**Figure 8(c)**).

4. RESULTS AND DISCUSSION

In **Figure 9**, the contour plot of the Von Mises stress in the tensile side of the Model A is reported for a bath characterised by a dipping time equal to 180s. The region in the plot is that across the symmetric axis over a length equal to about 1mm. Different values of the half bending angle are considered and more precisely: 1°, 2°, 4°, 6°, 12°, 20°, 25° and 32°. In **Figure 10** such a contour plot is reported for the Model B. The following values of the half-bending angle are considered and more precisely: 1°, 2°, 4°, 6°, 11°, 21°, 25° and 33°.

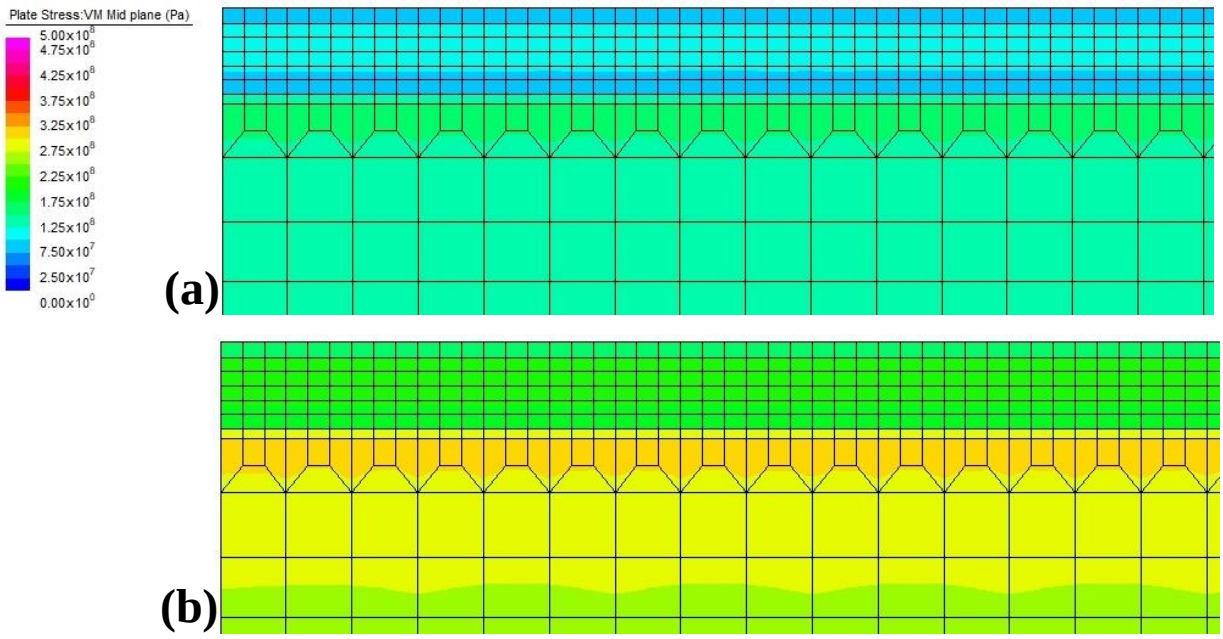

Continued

(c)

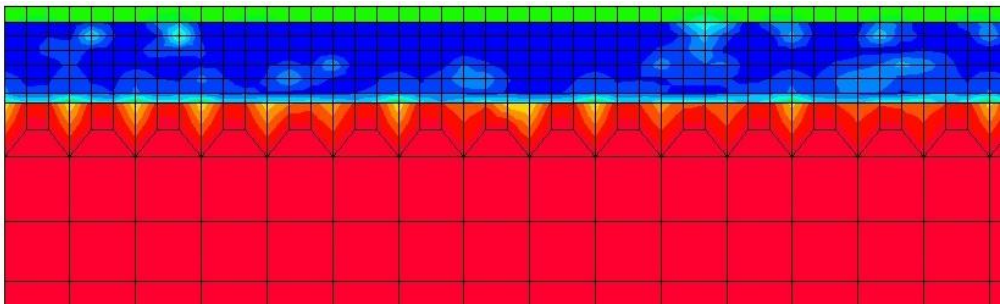

(d)

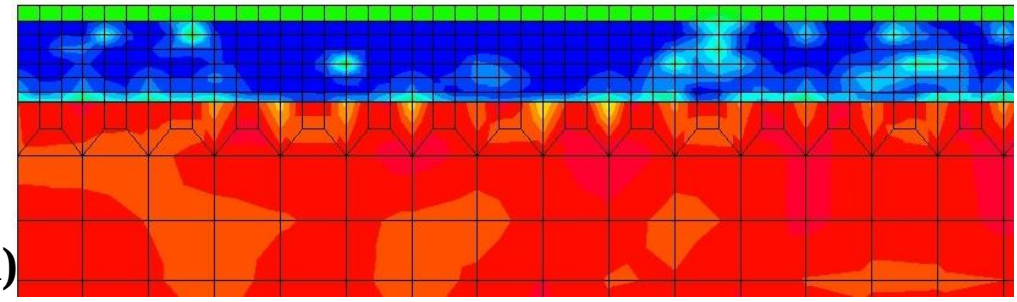

(e)

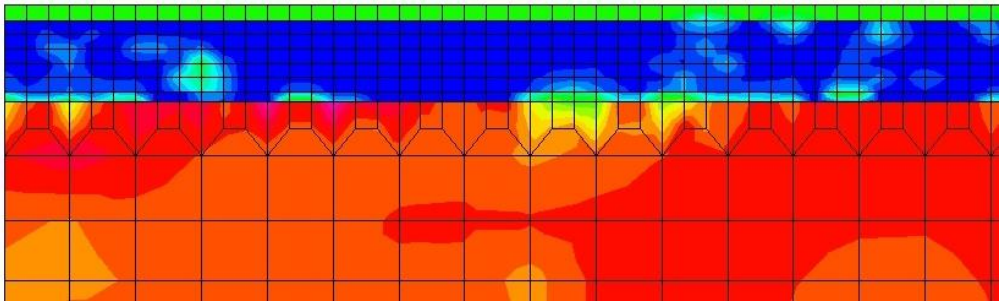

(f)

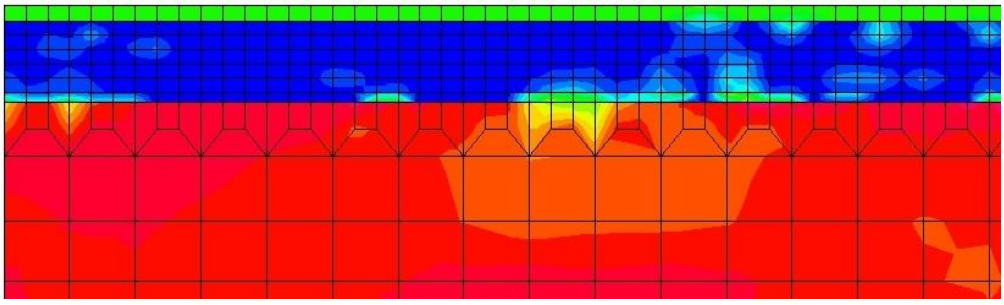

(g)

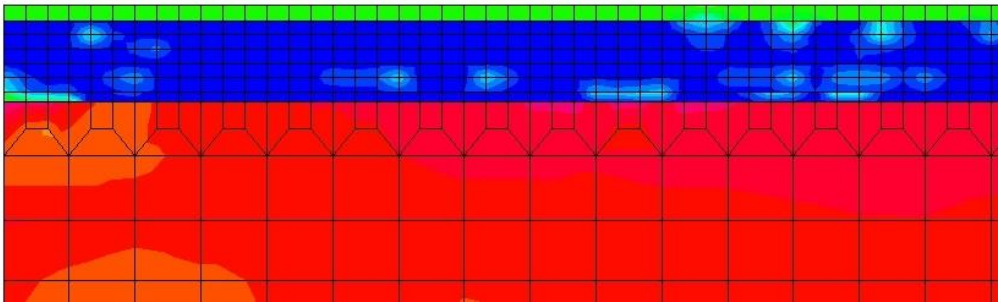

Continued

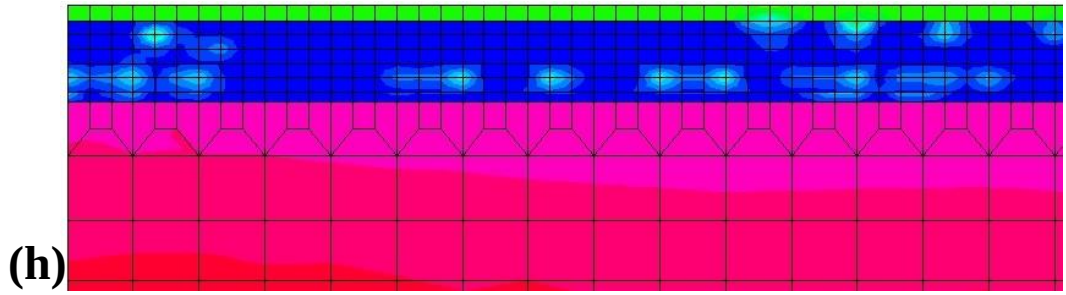

Figure 9. Pure zinc coating (dipping time 180s). Von Mises stress field at different values of the half bending angle, that is: (a) 1°, (b) 2°, (c) 4°, (d) 6°, (e) 12°, (f) 20°, (g) 25° and (h) 32°. The contour plot is related to the region across the symmetry axis and over a length equal to about 1.0mm.

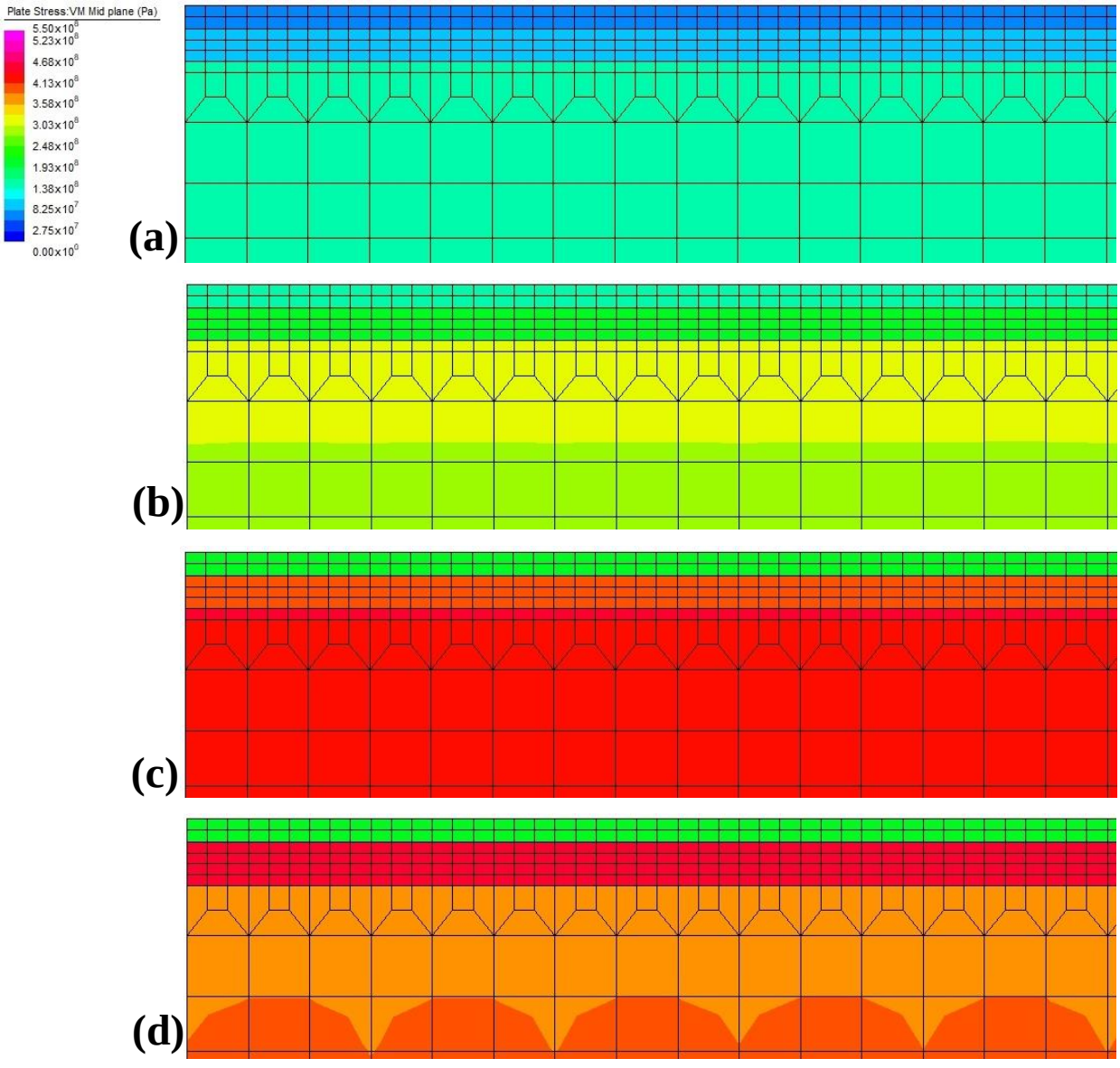

Continued

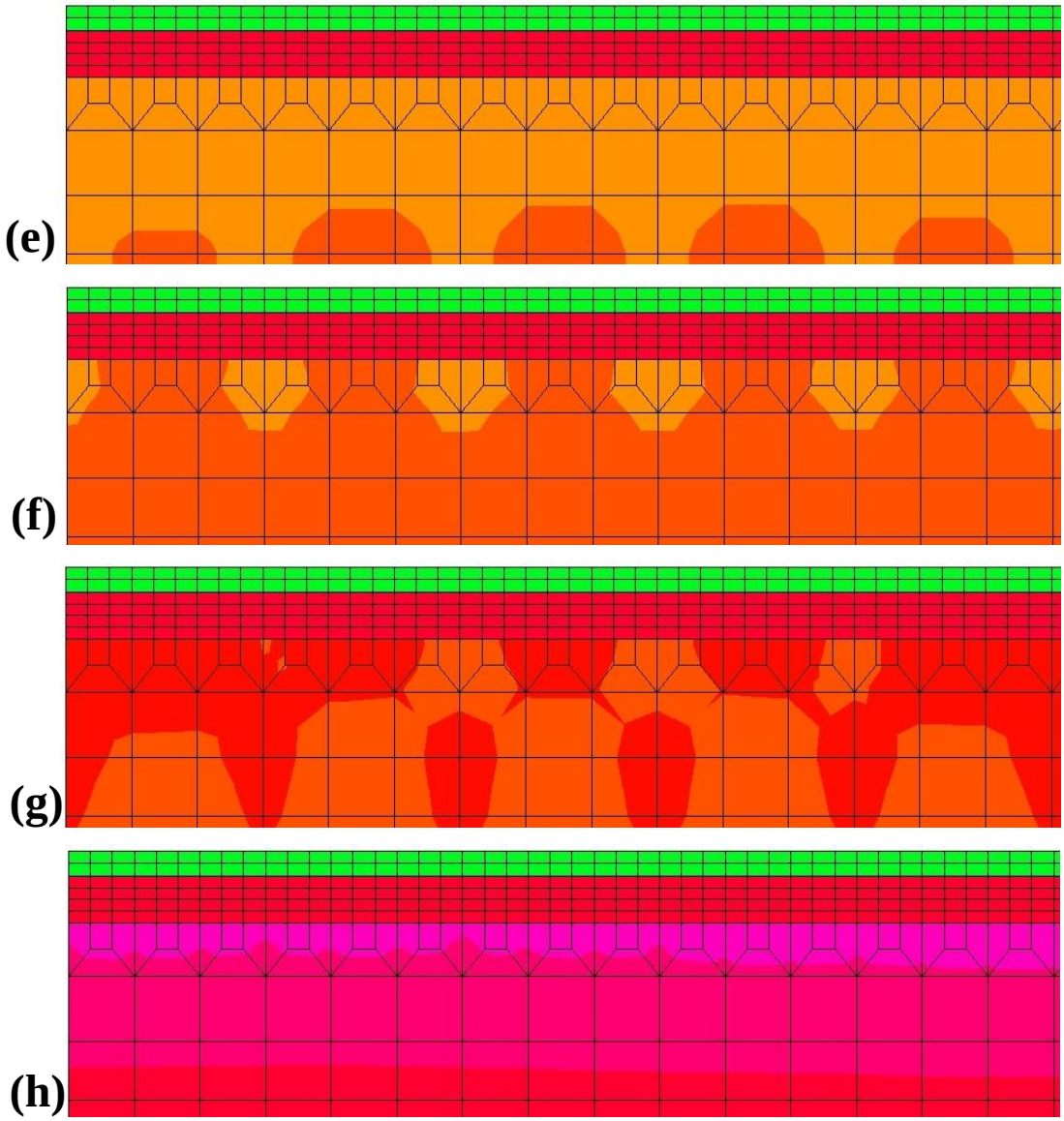

Figure 10. Zinc-based coating (dipping time 180s). Von Mises stress field at different values of the half bending angle, that is: (a) 1°, (b) 2°, (c) 4°, (d) 6°, (e) 11°, (f) 21°, (g) 25° and (h) 33°. The contour plot is related to the region across the symmetry axis and over a length equal to about 1.0mm.

In **Figure 11**, the results obtained by using the Model A, in terms of bending moment against the half bending angle, are shown for each bath examined and compared with the experimental results, whereas the results obtained from Model B are shown in **Figure 12**.

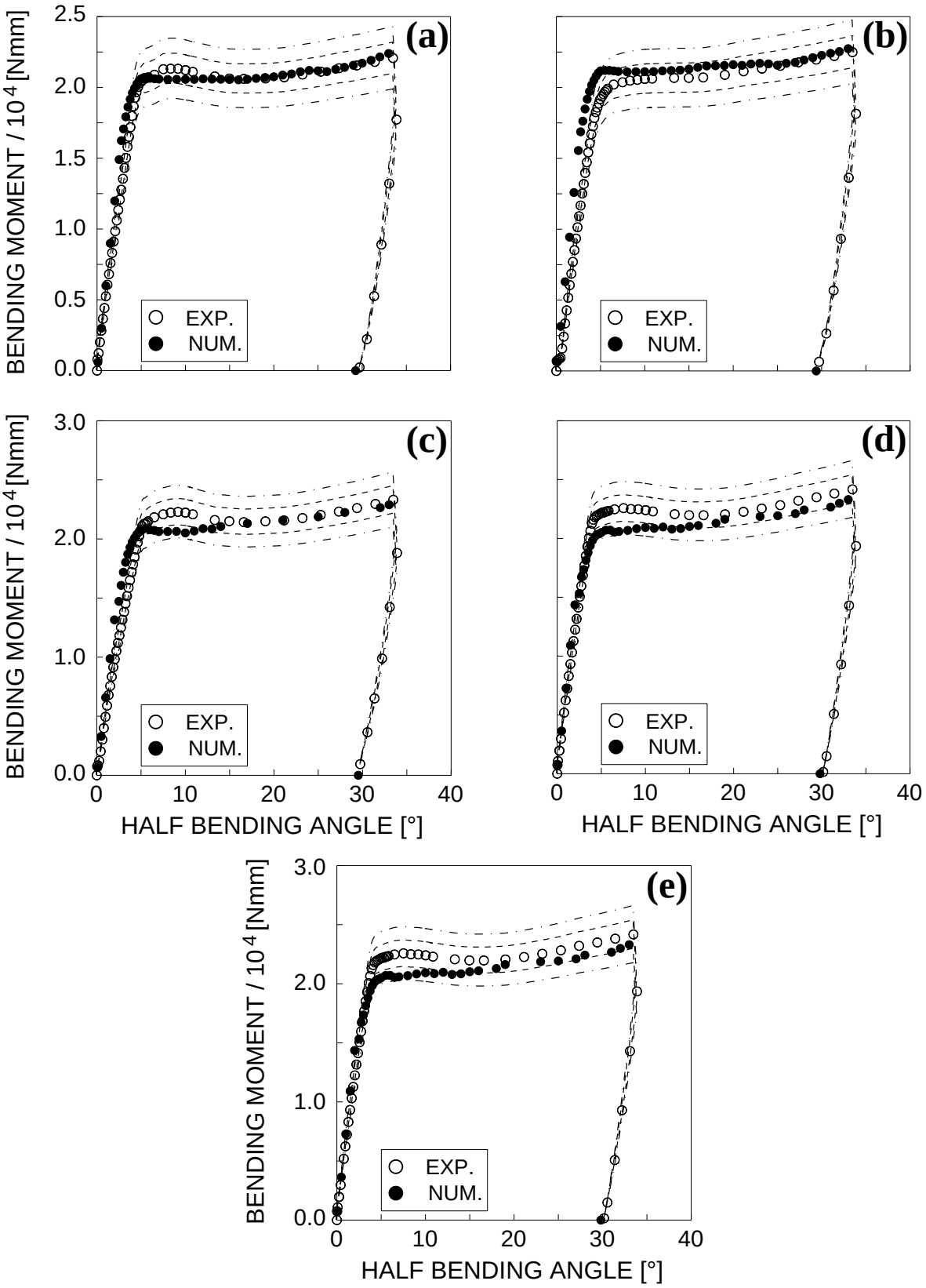

Figure 11. Numerical bending moment vs. half bending angle in the case of the pure zinc coating simulation at the dipping time of: (a) 15s, (b) 60s, (c) 180s, (d) 360s and (e) 900s. The experimental data are also reported.

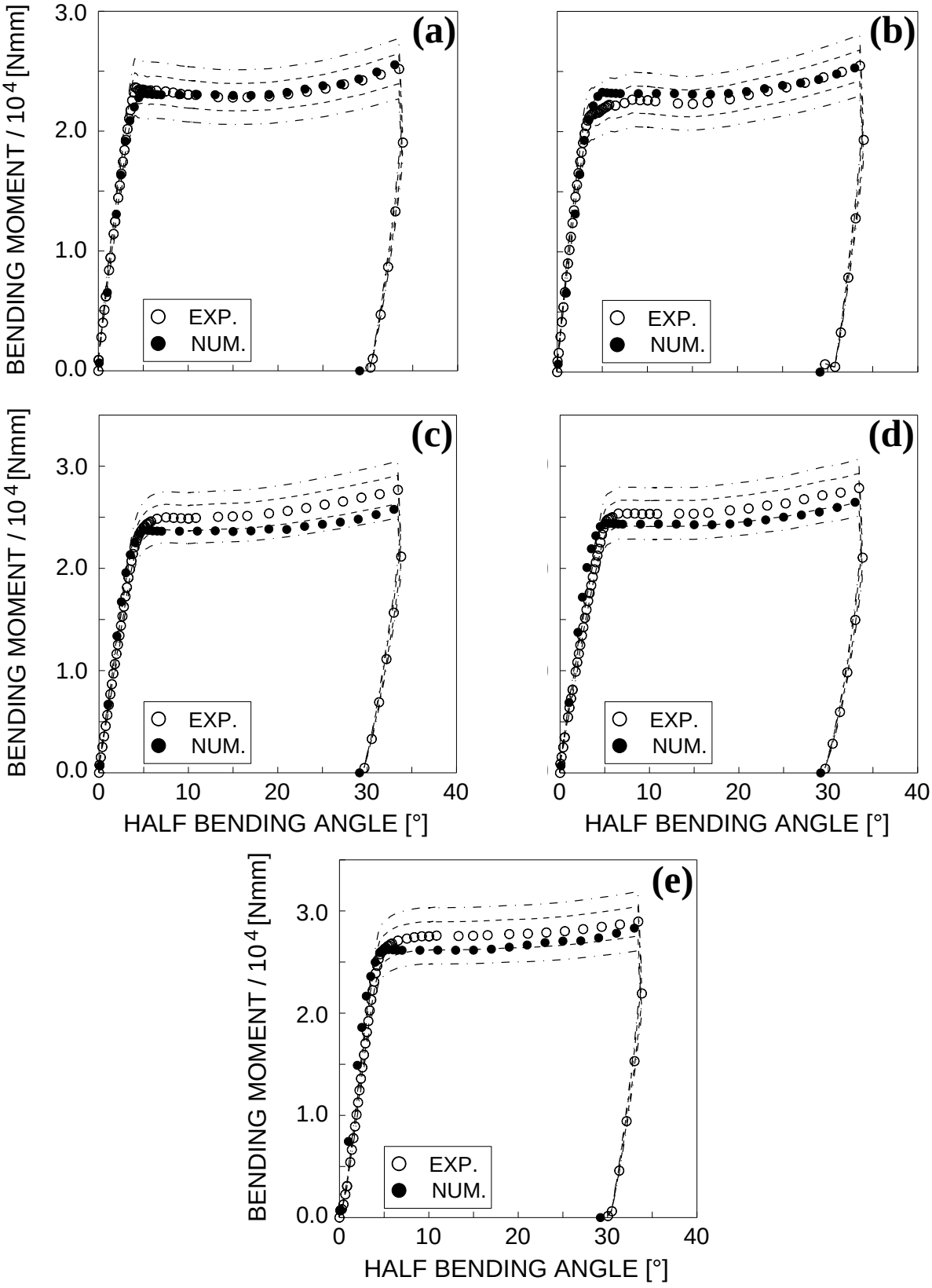

Figure 12. Numerical bending moment vs. half bending angle in the case of the technological coating simulation at the dipping time of: (a) 15s, (b) 60s, (c) 180s, (d) 360s and (e) 900s. The experimental data are also reported.

Note that, in such Figures, the dashed lines define an error equal to ±5% computed with respect to the value of the experimental bending moment, whereas the dash-dotted lines define an error equal to ±10%.

Relatively to the pure zinc bath simulations, it can be observed that:

- for a given value of the half bending angle, the numerical bending moment overestimates the corresponding experimental one in the elastic regime;
- the numerical bending moment does not exceed the ±10% of the corresponding experimental value from half bending angles greater than about 4°, that is in the plastic regime.

Relatively to the technological bath simulations, it can be observed that:

- for the dipping times equal to 15s and 60s, the slope of the elastic branch is quite well simulated by the numerical Model B;
- for the dipping times equal to 180s, 360s and 900s, and for a given value of the half bending angle, the numerical bending moment overestimates the corresponding experimental one in the elastic regime;
- the numerical bending moment does not exceed the ±10% of the corresponding experimental value from half-bending angles greater than about 3°, that is in the plastic regime.

5. CONCLUSIONS

In the present paper, the bending behaviour of a HD galvanised hot-rolled hyper-sandelin steel has been numerically simulated. Two

coating types have been considered and more precisely: a pure zinc coating and a zinc-based coating with 3% Sn addition by weight.

As it was experimentally observed, the above coatings are characterised by a different mechanical behaviour under bending, with an increase in flexural strength in the case of technological coating, for each dipping time examined. As a matter of fact, although the tin addition influences the thickness of each intermetallic phases, the better performance in terms of flexural strength is due to the increased ductility of the intermetallic phases.

Therefore, the key of the numerical simulation has been to assume suitable constitutive laws to phase layers, by considering that only few mechanical parameters are available in the literature, especially for the technological coating here examined. Therefore, such an assignment has been derived mainly from considerations on both the physical phenomenon of the interdiffusion between Zn and Fe atoms, and on the metallographies of the tensile side of the specimens.

Such an approach has shown quite satisfactory results. As a matter of fact, in general, although for a given value of the half bending angle the numerical bending moment overestimates the corresponding experimental one in the elastic regime, such a moment does not exceed the ±10% of the corresponding experimental value from half bending angles greater than about 3°-4°, that is in the plastic regime.

The numerical models developed have been able to capture also the experimental finding that only δ and ζ phases were damaging, whereas the η phase did not show any radial cracks.

Such an approach can be promising as a numerical tool to be used by HDG industry, being quite simple but quite accurate to estimate flexural strength and damaging of Zn-based coated steels.

Acknowledgements

The research work of Sabrina Vantadori and Andrea Zanichelli is supported by Italian Ministry of University and Research (P.R.I.N. National Grant 2017, Project code 2017HFPKZY; University of Parma Research Unit).

APPENDIX A

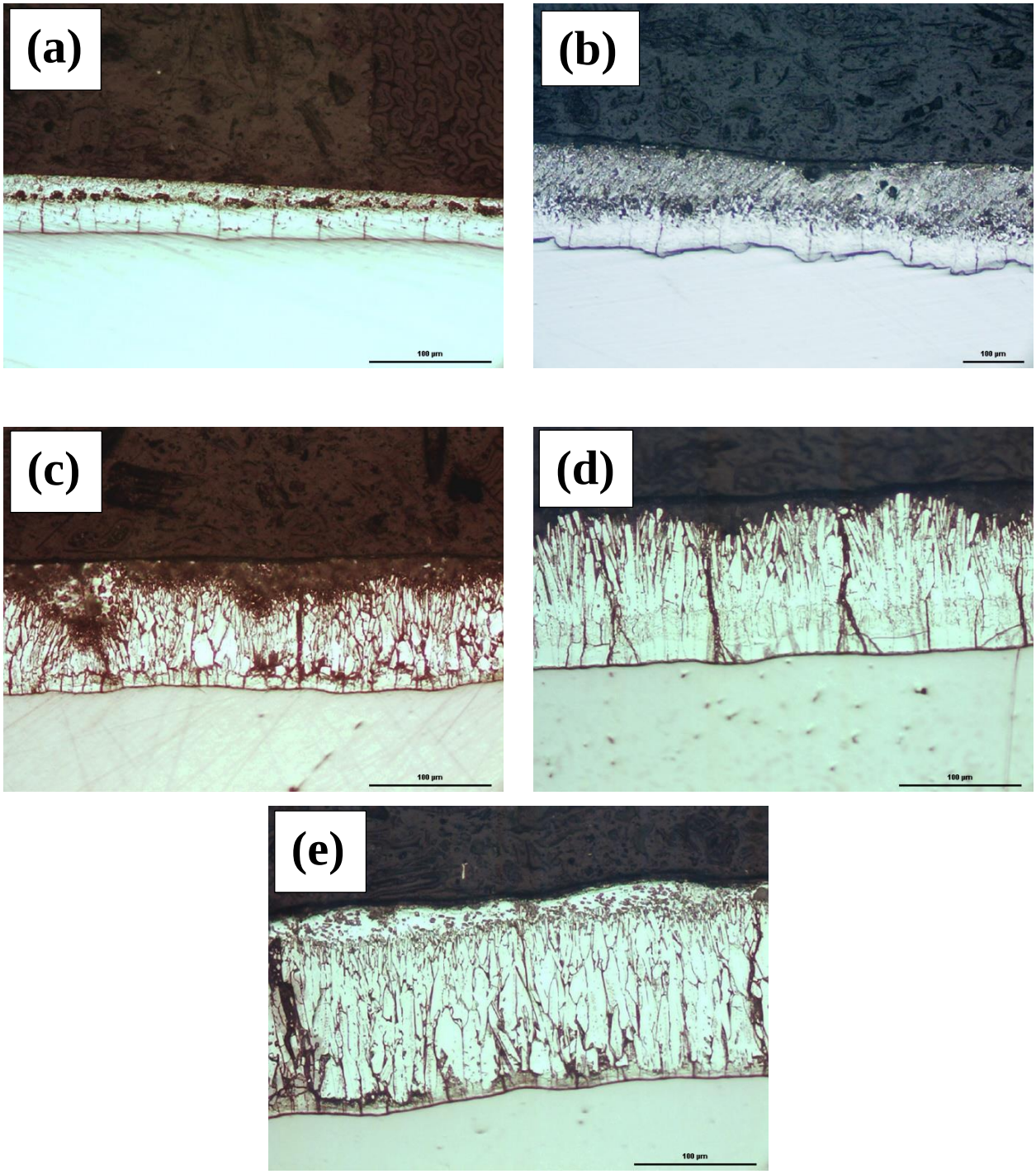

Figure A.1. Tensile side of the specimen in the case of the pure zinc bath at the dipping time of: (a) 15s, (b) 60s, (c) 180s, (d) 360s and (e) 900s.

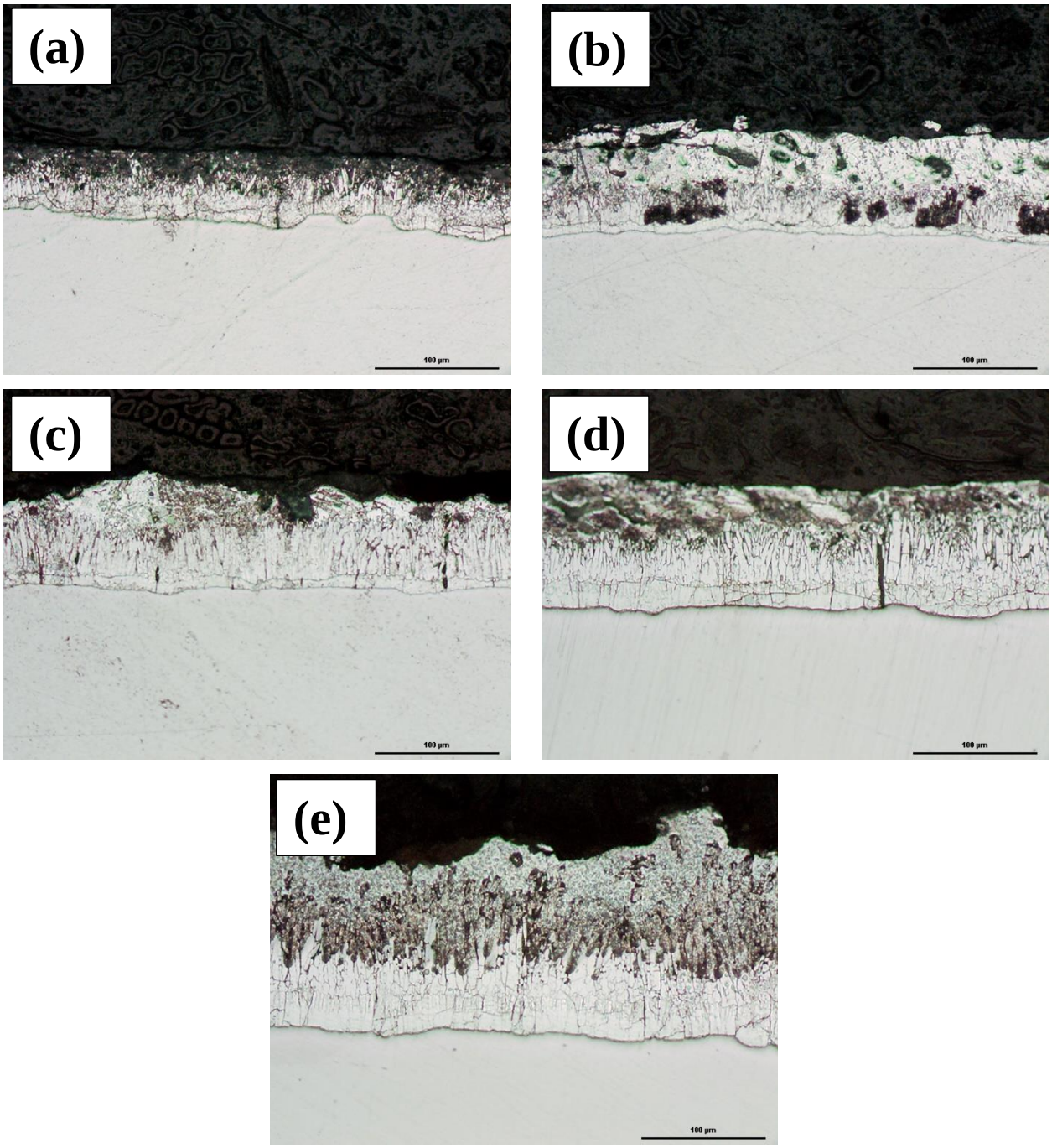

Figure A.2. Tensile side of the specimen in the case of the technological bath at the dipping time of: (a) 15s, (b) 60s, (c) 180s, (d) 360s and (e) 900s.

REFERENCES

[1] De Abreu Y., Da Silva A., Ruiz A., Réquiz R., Angulo N., Alanis R., Study of zinc coatings on steel substrate attained by two different techniques, Surface and Coatings Technology, 1999: 121; 120-, 682-686.
[2] L. Jintang, C. Chunshan, K. Gang, X. Qiaoyu, C. Jinhong, Influence of silicon on the a-Fe/U interface of hot dip galvanized steels, Surface and Coatings Technology 2006: 200; 5277–5281.
[3] Razavi S.M.J., Peron M., Torgersen J., Berto F., Mutignani F., Effect of hot dip galvanization on the fatigue strength of steel bolted connections, Frattura ed Integrita Strutturale, 2017; 11: 432-439.
[4] Huang X.-G., Wang Z.-Q., Durability method on corrosion fatigue performance of AH 32 steel, Frattura ed Integrita Strutturale, 2019; 13: 481-490.
[5] UNI EN ISO 1461, Hot dip galvanized coatings on fabricated iron and steel articles — Specifications and test methods, 2009.
[6] Di Cocco V., Iacoviello F., D'Agostino L., Natali S. Damage micromechanisms in a hot dip galvanized steel, Procedia Structural Integrity, 2017; 3: 231-236.
[7] Tzimas E., Papadimitrou G., Cracking mechanisms in high temperature hot-dip galvanised coatings, Surface and Coatings Technology, 2001; 145: 176-185.
[8] Marder A.R., A review of the metallurgy of zinc coated steel, Progress in Materials Science, 2000; 45: 191–198.
[9] Reumont G., Voct J.B., Iost A., Foct J., The effects of an Fe-Zn intermetallic-containing coating on the stress corrosion cracking behaviour of a hot-dip galvanised steel, Surface and coatings technology, 2001; 139: 265-271.
[10] Duncan J.L., Ding S.-C., Jiang W.L., Moment-curvature measurement in thin sheet-part I: equipment. International Journal of Mechanical Sciences, 1999; 41: 249-260.
[11] Di Cocco V., Iacoviello F., Iacoviello D. Image processing approach in Zn-Ti-Fe kinetic phase evaluation. Computational Modelling of Objects Represented in Images: Fundamentals, Methods and Applications III - Proceedings of the International Symposium, CompIMAGE 2012, pp. 421-426.
[12] Chen, J., Effect of Ni and Co in zinc bath on thickness and microstructure of hot-dip galvanized coating on high Si-contained steel, Heat Treatment of Metals,
2012: 37; 110-114.
[13] Pistofidis N., Vourlias G., Pavlidou E., Stergioudis G., Effect of Ti, Ni and Bi addition to the corrosion resistance of Zn hot-dip galvanized coatings, Journal of Optoelectronics and Advanced Materials, 2007; 9: 1653-1659.
[14] Kania H., Liberski P., Synergistic influence of the addition of Al, Ni and Pb to a zinc bath upon growth kinetics and structure of coatings, Solid State Phenomena, 2014; 212: 115-120.
[15] Chakraborty A., Govardhana P., Mondal A., Laha T., Dutta M., Singh S.B. Microstructural development of prior nickel coated hot

dipped galvanised coatings, Journal of Alloys and Compounds, 2017; 699: 648-656.
[16] Vagge S.T., Raja V.S., Influence of strontium on electrochemical corrosion behavior of hot-dip galvanized coating, Surface and coatings technology, 2009; 203: 3092–3098.
[17] Shibli S.M.A., Manu R., Development of zinc oxide-rich inner layers in hot-dip zinc coating for barrier protection, Surface and coatings technology, 2006; 201: 2358-2363.
[18] Di Cocco V., Iacoviello F., Natali S., Cracking mechanisms in a hot-dip zinc coated steel, 11th International Conference on Fracture 2005, ICF11, 2005; 6: 4076-4080.
[19] Di Cocco V., Iacoviello F., Natali S.Damaging micromechanisms in hot-dip galvanizing Zn based coatings, Theoretical and Applied Fracture Mechanics, 2014; 70: 91-98.
[20] Di Cocco V., Iacoviello F., D'Agostino L., Natali S., Sn and Ti influence on damage of bent hot-dip galvanizing phases, Procedia Structural Integrity, 2017; 3: 224-230.
[21] Carpinteri A., Di Cocco V., Fortese G., Iacoviello F., Natali S., Ronchei C., Scorza D., Vantadori S., Kinetics of Intermetallic Phases and Mechanical Behavior of ZnSn3% Hot-Dip Galvanization Coatings, Advanced Engineering Materials, 2016; 18: 2088-2094.
[22] Kim S.-R., Nairn J.A., Fracture mechanics analysis of coating/substrate systems. Part I: Analysis of tensile and bending exeriments, Engineering Fracture Mechanics, 2000; 65: 573-593.
[23] Kim S.-R., Nairn J.A., Fracture mechanics analysis of coating/substrate systems. Part II: Experiments in bending, Engineering Fracture Mechanics, 2000; 65: 595-607.